

Aims and Scope. *JGR: Atmospheres* publishes articles that advance and improve understanding of atmospheric properties and processes, including the interaction of the atmosphere with other components of the Earth system.

Editors: Minghua Zhang (Editor-in-Chief), (minghua.zhang@stonybrook.edu), (<http://orcid.org/0000-0002-1927-5405>), James H. Crawford, Ulrike Langematz, Zhanqing Li, Ruby Leung, Lynn Russell, Allison Steiner, Chidong Zhang (<http://orcid.org/0000-0001-9708-1561>).

Associate Editors: David Atkinson, Kristie A. Boering, Simon A. Carn, Jens Hesselbjerg Christensen, Anthony B. Davis, Neil Donahue, Xiquan Dong, Gregory J. Frost, Joe Galewsky, Matei Georgescu, Mitchell D. Goldberg, Diego Janches, Jonathan Jiang, Ben P. Kirtman, Pavlos Kollias, Robert Levy, Chuntao Liu, Guosheng Liu, Yangang Liu, Jens Oberheide, Victor Pasko, Wouter Peters, Colin Price, Thomas Reddman, Yinon Rudich, David Simpson, Ivanka Stajner, Ina Tegen, Kaicun Wang, Minghui Wang, Tao Wang, Martin Wild, David Winker, Zhenghui Xie, Xiu-Qun Yang, Francis Zwiers.

AGU Editorial Team. For assistance with submitted manuscripts, file specifications, or AGU publication policy please contact jgr-atmospheres@agu.org.

For submission instructions or to submit a manuscript visit: <http://jgr-atmospheres-submit.agu.org>.

The journal to which you are submitting your manuscript employs a plagiarism detection system. By submitting your manuscript to this journal you accept that your manuscript may be screened for plagiarism against previously published works.

JGR: Atmospheres accepts articles for Open Access publication. Please visit <http://olabout.wiley.com/WileyCDA/Section/id-406241.html> for further information about OnlineOpen.

Publication Charges. The publication charge income received for *JGR: Atmospheres* helps support rapid publication, allows more articles per volume, makes possible the low subscription rates, and supports many of AGU's scientific and outreach activities. Publication charge information can be found here: <http://publications.agu.org/author-resource-center/publication-fees/>.

To encourage papers to be written in a concise fashion, there is an excess length fee. For *JGR: Atmospheres* the fee is assessed only on the equivalent of more than 25 publication units. The excess length fee does not apply to review articles, and the editor may waive the fee on a limited number of concisely written papers that merit being longer. There is no charge for color in any format.

Copyright and Photocopying. Copyright © 2016. American Geophysical Union. All rights reserved. No part of this publication may be reproduced, stored or transmitted in any form or by any means without the prior permission in writing from the copyright holder. Authorization to copy items for internal and personal use is granted by the copyright holder for libraries and other users registered with their local Reproduction.

Cover: *Li et al.* [DOI: [10.1002/2016JD025252](https://doi.org/10.1002/2016JD025252)] investigated mixing structure of individual particles at Mount Tai as cloud/fog air, Greater Khingan as clean background air, biomass burning and coal burning as emission sources, urban and suburban area as polluted air, and rural site as polluted background air. Within the internally-mixed particle class, we identified four heterogeneous mixing structures: core-shell, dumbbell, OM-coating, and dispersed-OM, as well as one homogeneous-like mixing structure. Particle mixing structures depend on particle size and location, and evolve with time and long-range transported particles tended to have core-shell and OM-coating structures. See pp. 13,784–13,798.

Rights Organization (RRO), e.g. Copyright Clearance Center (CCC), 222 Rosewood Drive, Danvers, MA 01923, USA (www.copyright.com), provided the appropriate fee is paid directly to the RRO. This consent does not extend to other kinds of copying such as copying for general distribution, for advertising or promotional purposes, for creating new collective works or for resale. Special requests should be addressed to: publications@agu.org.

Disclaimer. The Publisher, American Geophysical Union, and Editors cannot be held responsible for errors or any consequences arising from the use of information contained in this journal; the views and opinions expressed do not necessarily reflect those of the Publisher, American Geophysical Union, and Editors, neither does the publication of advertisements constitute any endorsement by the Publisher, American Geophysical Union, and Editors of the products advertised.

Individual Subscriptions. Member subscriptions are available through members.agu.org or by contacting the AGU Member Service Center. The Service Center is open from 8:00 a.m. to 8:30 p.m. Eastern time: +1 202 462 6900, +1 800 966 2481; Fax: +1 202 777 7393; e-mail: service@agu.org. Questions about meetings or membership will be referred to the appropriate staff.

Publisher. *JGR: Atmospheres* is published on behalf of the American Geophysical Union by Wiley Periodicals, Inc., 111 River St., Hoboken, NJ, 07030-5774, +1 201 748 6000.

Journal Customer Services. For institutional subscription information, claims and any enquiry concerning your journal subscription please go to www.wileycustomerhelp.com/ask or contact your nearest office.

Americas: Email: cs-journals@wiley.com; Tel: +1 781 388 8598 or +1 800 835 6770 (toll free in the USA & Canada).

Europe, Middle East and Africa: Email: cs-journals@wiley.com; Tel: +44 (0) 1865 778315.

Asia Pacific: Email: cs-journals@wiley.com; Tel: +65 6511 8000.

Japan: For Japanese speaking support, Email: cs-japan@wiley.com; Tel: +65 6511 8010 or Tel (toll-free): 005 316 50 480.

Visit our Online Customer Help available in 7 languages at www.wileycustomerhelp.com/ask.

Production Editor. For assistance with post-acceptance articles and other production issues please contact JGRDprod@wiley.com.

Access to this journal is available free online within institutions in the developing world through the AGORA initiative with the FAO, the HINARI initiative with the WHO, the OARE initiative with UNEP, and the ARDI initiative with WIPO. For information, visit www.aginternetwork.org, www.who.int/hinari/en/, www.oaresciences.org, or www.wipo.int/ardi/en.

ISSN 2169-8996 (Online)

View this journal online at <http://jgr-atm.agu.org>.

Climate and Dynamics

- 13,207** *A. Barkhordarian, H. von Storch, E. Zorita, and J. J. Gómez-Navarro*
An attempt to deconstruct recent climate change in the Baltic Sea basin (doi 10.1002/2015JD024648)
- 13,218** *Nathaniel W. Chaney, Jonathan D. Herman, Michael B. Ek, and Eric F. Wood*
Deriving global parameter estimates for the Noah land surface model using FLUXNET and machine learning (doi 10.1002/2016JD024821)
- 13,236** *Sally L. Lavender and Andrew J. Dowdy*
Tropical cyclone track direction climatology and its intraseasonal variability in the Australian region (doi 10.1002/2016JD025562)
- 13,250** *Yang Zhou, Youyu Lu, Ben Yang, Jing Jiang, Anning Huang, Yong Zhao, Mengke La, and Qing Yang*
On the relationship between the Madden-Julian Oscillation and 2 m air temperature over central Asia in boreal winter (doi 10.1002/2016JD025651)
- 13,273** *Bradford S. Barrett, Elizabeth R. Sanabia, Sara C. Reynolds, Julie K. Stapleton, and Anthony L. Borrego*
Evolution of the upper tropospheric outflow in Hurricanes Iselle and Julio (2014) in the Navy Global Environmental Model (NAVEM) analyses and in satellite and dropsonde observations (doi 10.1002/2016JD025656)
- 13,287** *Ashley E. Payne and Gudrun Magnusdottir*
Persistent landfalling atmospheric rivers over the west coast of North America (doi 10.1002/2016JD025549)
- 13,301** *Jessica Keune, Fabian Gasper, Klaus Goergen, Andreas Hense, Prabhakar Shrestha, Mauro Sulis, and Stefan Kollet*
Studying the influence of groundwater representations on land surface-atmosphere feedbacks during the European heat wave in 2003 (doi 10.1002/2016JD025426)
- 13,326** *Thomas J. Aubry, A. Mark Jellinek, Wim Degruyter, Costanza Bonadonna, Valentina Radić, Margot Clyne, and Adjoa Quainoo*
Impact of global warming on the rise of volcanic plumes and implications for future volcanic aerosol forcing (doi 10.1002/2016JD025405)
- 13,352** *Acacia S. Pepler, Lisa V. Alexander, Jason P. Evans, and Steven C. Sherwood*
The influence of local sea surface temperatures on Australian east coast cyclones (doi 10.1002/2016JD025495)
- 13,364** *Matthew Garcia and Philip A. Townsend*
Recent climatological trends and potential influences on forest phenology around western Lake Superior, USA (doi 10.1002/2016JD025190)
- 13,392** *Daniel A. Rajewski, Eugene S. Takle, John H. Prueger, and Russell K. Doorenbos*
Toward understanding the physical link between turbines and microclimate impacts from in situ measurements in a large wind farm (doi 10.1002/2016JD025297)
- 13,415** *A. Creese and R. Washington*
Using qflux to constrain modeled Congo Basin rainfall in the CMIP5 ensemble (doi 10.1002/2016JD025596)
- 13,443** *Hoffman H. N. Cheung, Wen Zhou, Marco Y. T. Leung, C. M. Shun, S. M. Lee, and H. W. Tong*
A strong phase reversal of the Arctic Oscillation in midwinter 2015/2016: Role of the stratospheric polar vortex and tropospheric blocking (doi 10.1002/2016JD025288)
- 13,458** *Hai Yan Li, Chun Ming Huang, Shao Dong Zhang, Kai Ming Huang, Yehui Zhang, Yun Gong, Quan Gan, and Yue Jia*
Low-frequency oscillations of the gravity wave energy density in the lower atmosphere at low latitudes revealed by U.S. radiosonde data (doi 10.1002/2016JD025435)
- 13,474** *S. Kalisch, H.-Y. Chun, M. Ern, P. Preusse, Q. T. Trinh, S. D. Eckermann, and M. Riese*
Comparison of simulated and observed convective gravity waves* (doi 10.1002/2016JD025235)
- *This article is part of a Special Section—Fast Physics in Climate Models: Parameterization, Evaluation and Observation
- 13,493** *M. Vázquez, R. Nieto, A. Drumond, and L. Gimeno*
Moisture transport into the Arctic: Source-receptor relationships and the roles of atmospheric circulation and evaporation* (doi 10.1002/2016JD025400)
- *This article is part of a Special Section—The Arctic: An AGU Joint Special Collection

Aerosol and Clouds

- 13,510** *S. J. O'Shea, T. W. Choullarton, G. Lloyd, J. Crosier, K. N. Bower, M. Gallagher, S. J. Abel, R. J. Cotton, P. R. A. Brown, J. P. Fugal, O. Schlenker, S. Borrmann, and J. C. Pickering*
Airborne observations of the microphysical structure of two contrasting cirrus clouds (doi 10.1002/2016JD025278)
- 13,537** *Li Xu, Philip Cameron-Smith, Lynn M. Russell, Steven J. Ghan, Ying Liu, Scott Elliott, Yang Yang, Sijia Lou, Maryam A. Lamjiri, and Manfredi Manizza*
DMS role in ENSO cycle in the tropics (doi 10.1002/2016JD025333)

- 13,559** *I. Steinke, R. Funk, J. Busse, A. Iturri, S. Kirchen, M. Leue, O. Möhler, T. Schwartz, M. Schnaiter, B. Sierau, E. Toprak, R. Ullrich, A. Ulrich, C. Hoese, and T. Leisner*
Ice nucleation activity of agricultural soil dust aerosols from Mongolia, Argentina, and Germany (doi 10.1002/2016JD025160)
- 13,577** *Bingqi Yi, Ping Yang, Quanhua Liu, Paul van Delst, Sid-Ahmed Boukabara, and Fuzhong Weng*
Improvements on the ice cloud modeling capabilities of the Community Radiative Transfer Model (doi 10.1002/2016JD025207)
- 13,591** *L. Carro-Calvo, C. Hoese, M. Stengel, and S. Salcedo-Sanz*
Cloud glaciation temperature estimation from passive remote sensing data with evolutionary computing (doi 10.1002/2016JD025552)
- 13,609** *Jing Li, Xichen Li, Barbara E. Carlson, Ralph A. Kahn, Andrew A. Lacis, Oleg Dubovik, and Teruyuki Nakajima*
Reducing multisensor satellite monthly mean aerosol optical depth uncertainty: 1. Objective assessment of current AERONET locations (doi 10.1002/2016JD025469)
- 13,628** *Yongjoo Choi and Young Sung Ghim*
Estimation of columnar concentrations of absorbing and scattering fine mode aerosol components using AERONET data (doi 10.1002/2016JD025080)
- 13,641** *Poonam Tyagi, Kimitaka Kawamura, Srinivas Bikkina, Tomoki Mochizuki, and Kazuma Aoki*
Hydroxy fatty acids in snow pit samples from Mount Tateyama in central Japan: Implications for atmospheric transport of microorganisms and plant waxes associated with Asian dust (doi 10.1002/2016JD025340)
- 13,661** *Taylor Shingler, Armin Sorooshian, Amber Ortega, Ewan Crosbie, Anna Wonaschütz, Anne E. Perring, Andreas Beyersdorf, Luke Ziemba, Jose L. Jimenez, Pedro Campuzano-Jost, Tomas Mikoviny, Armin Wisthaler, and Lynn M. Russell*
Ambient observations of hygroscopic growth factor and $f(\text{RH})$ below 1: Case studies from surface and airborne measurements* (doi 10.1002/2016JD025471)
- *This article is part of a Special Section—Studies of Emissions and Atmospheric Composition, Clouds and Climate Coupling by Regional Surveys, 2013 (SEAC4RS)
- 13,678** *C. D. Groot Zwaftink, H. Grythe, H. Skov, and A. Stohl*
Substantial contribution of northern high-latitude sources to mineral dust in the Arctic (doi 10.1002/2016JD025482)
- 13,698** *Erica K. Dolinar, Xiquan Dong, Baike Xi, Jonathan H. Jiang, and Norman G. Loeb*
A clear-sky radiation closure study using a one-dimensional radiation transfer model and collocated satellite-surface-reanalysis data sets (doi 10.1002/2016JD025823)
- 13,715** *Christina Kalb, Wiebke Deierling, Andreas Baumgaertner, Michael Peterson, Chuntao Liu, and Douglas Mach*
Parameterizing total storm conduction currents in the Community Earth System Model (doi 10.1002/2016JD025376)
- 13,735** *Wenhua Gao, Chung-Hsiung Sui, Jiwen Fan, Zhiqun Hu, and Lingzhi Zhong*
A study of cloud microphysics and precipitation over the Tibetan Plateau by radar observations and cloud-resolving model simulations (doi 10.1002/2015JD024196)
- Composition and Chemistry**
- 13,753** *Matthew S. Johnson, Xin Xi, Seongeun Jeong, Emma L. Yates, Laura T. Iraci, Tomoaki Tanaka, Max Loewenstein, Jovan M. Tadić, and Marc L. Fischer*
Investigating seasonal methane emissions in Northern California using airborne measurements and inverse modeling (doi 10.1002/2016JD025157)
- 13,768** *Timothy P. Canty, Ross J. Salawitch, and David M. Wilmouth*
The kinetics of the ClOOCl catalytic cycle (doi 10.1002/2016JD025710)
- 13,784** *Weijun Li, Jiaying Sun, Liang Xu, Zongbo Shi, Nicole Riemer, Yele Sun, Pingqing Fu, Jianchao Zhang, Yangting Lin, Xinfeng Wang, Longyi Shao, Jianmin Chen, Xiaoye Zhang, Zifa Wang, and Wenxing Wang*
A conceptual framework for mixing structures in individual aerosol particles (doi 10.1002/2016JD025252)

RESEARCH ARTICLE

10.1002/2016JD025252

Key Points:

- Our study systematically identifies mixing structures within internally mixed particles
- Particle mixing structures depend on particle size and location and they evolve over time
- Secondary aerosol formation mainly determined particle mixing structures in this study

Supporting Information:

- Supporting Information S1

Correspondence to:

W. Li,
liweijun@sdu.edu.cn

Citation:

Li, W., et al. (2016), A conceptual framework for mixing structures in individual aerosol particles, *J. Geophys. Res. Atmos.*, 121, 13,784–13,798, doi:10.1002/2016JD025252.

Received 21 APR 2016

Accepted 4 NOV 2016

Accepted article online 7 NOV 2016

Published online 25 NOV 2016

A conceptual framework for mixing structures in individual aerosol particles

Weijun Li¹, Jiaxing Sun¹, Liang Xu¹, Zongbo Shi², Nicole Riemer³, Yele Sun⁴, Pingqing Fu⁴, Jianchao Zhang⁵, Yangting Lin⁵, Xinfeng Wang¹, Longyi Shao⁶, Jianmin Chen¹, Xiaoye Zhang⁷, Zifa Wang⁴, and Wenxing Wang¹

¹Environment Research Institute, Shandong University, Jinan, China, ²School of Geography, Earth and Environmental Sciences, University of Birmingham, Birmingham, UK, ³Department for Atmospheric Sciences, University of Illinois at Urbana-Champaign, Champaign, Illinois, USA, ⁴State Key of Laboratory of Atmospheric Boundary Physics and Atmospheric Chemistry, Institute of Atmospheric Physics, Chinese Academy of Sciences, Beijing, China, ⁵Key Laboratory of Earth and Planetary Physics, Institute of Geology and Geophysics, Chinese Academy of Sciences, Beijing, China, ⁶State Key Laboratory of Coal Resources and Safe Mining, China University of Mining and Technology, Beijing, China, ⁷Key Laboratory of Atmospheric Chemistry, Chinese Academy of Meteorological Sciences, Beijing, China

Abstract This study investigated the particle size- and age-dependent mixing structures of individual particles in clean and polluted air. Aerosols were classified into eight components: sea salt, mineral dust, fly ash, metal, soot, sulfates, nitrates, and organic matter (OM). Based on our aerosol classification, a particle that consists of two or more aerosol components can be defined as an internally mixed particle. Otherwise, it is considered to be an externally mixed particle. Within the internally mixed particle class, we identified four heterogeneous mixing structures: core-shell, dumbbell, OM coating, and dispersed OM, as well as one homogeneous-like mixing structure. Homogeneous-like mixing mainly occurred in fine particles (<1 μm), while the frequency of heterogeneously mixed particles increased with particle size. Our study demonstrated that particle mixing structures depend on particle size and location and evolve with time. OM-coating and core-shell structures are important indicators for particle aging in air as long as they are distant from specific emission sources. Long-range transported particles tended to have core-shell and OM-coating structures. We found that secondary aerosol components (e.g., sulfates, nitrates, and organics) determined particle mixing structures, because their phases change following particle hydration and dehydration under different relative humidities. Once externally mixed particles are transformed into internally mixed particles, they cannot revert to their former state, except when semivolatile aerosol components are involved. Categorizing mixing structures of individual particles is essential for studying their optical and hygroscopic properties and for tracing the development of their physical or chemical properties over time.

1. Introduction

Atmospheric particles often contain sulfate, ammonium, nitrate, elemental carbon, organic compounds, trace metals, crustal elements, and water. Particle composition, size, and morphology are of great importance for determining aerosol impacts on health, visibility, climate, and cloud formation [Buseck and Posfai, 1999; Jacobson, 2001; McFiggans et al., 2006; Moffet and Prather, 2009; Gieré and Querol, 2010]. Here we use “morphology” to refer to the individual aerosol particle’s shape in the atmosphere. A term that is often used to describe the complex mixtures of chemical constituents within aerosol populations is the “aerosol mixing state,” and different interpretations of this term prevail within the community. Here we emphasize the contrast between the “population mixing state” and the “mixing state of an individual particle.” Riemer and West [2013] defined the population mixing state as the distribution of the aerosol chemical species among the particles in a given population. They proposed the mixing state index χ as an appropriate metric to quantify the population mixing state, ranging from 0 for a completely external mixture where particles consist of a single species to 1 for a completely internal mixture, where the per-particle composition is identical to the composition of the bulk aerosol. It is important to note that the population mixing state metrics are purely based on per-particle composition and that the morphology and composition of individual particles do not enter into this definition. In contrast, the mixing state of an individual particle is focused on the distribution of aerosol components within and on its surface; hence, the morphology of the particle helps define its mixing state.

The mixing state of an individual particle is expected to affect its optical and hygroscopic properties through numerous physical and chemical processes that alter particle composition during aerosol transport in the troposphere [Jacobson, 2001; Lesins et al., 2002; Fuzzi et al., 2006; Zhang et al., 2008]. Therefore, details on its mixing state, such as the state of aggregation, the existence of eccentric inclusions, or the presence of concentric layers of different aerosol components, are essential elements that can bridge field and laboratory studies in atmospheric chemistry. For example, nitrate coatings on aged mineral dust and sea salt particles have been explored in numerous laboratory experiments [Laskin et al., 2005; Gibson et al., 2006; Liu et al., 2007; Li and Shao, 2009b; Chi et al., 2015]. Therefore, the knowledge of mixing state is crucial for modeling studies; from it, one can infer the hygroscopic and optical properties of particles, providing information about their aging, reaction histories, and sources.

Many studies have described quantitative techniques for assessing the mixing state of aerosol particles [Adachi and Buseck, 2008; Shiraiwa et al., 2008; Zelenyuk et al., 2008; Moffet and Prather, 2009; Oshima et al., 2009; Anttila, 2010; Dall'Osto et al., 2010; Deboudt et al., 2010; Geng et al., 2010; Li and Shao, 2010; Pratt and Prather, 2010; Cheng et al., 2012; Riemer and West, 2013; Zhang et al., 2013; Li et al., 2014b]. There are several experimental techniques for probing different aspects of the aerosol mixing state, including single-particle analysis, chemical analysis techniques for size-resolved aerosol mass, Single Particle Laser Ablation Time-of-Flight Mass Spectrometer [Zelenyuk et al., 2008], aerosol time-of-flight mass Spectrometer (ATOFMS) [Moffet and Prather, 2009; Dall'Osto et al., 2010; Pratt and Prather, 2010; Zhang et al., 2013; Healy et al., 2014], scanning and transmission electron microscopy (SEM/TEM) [Buseck and Posfai, 1999; Adachi and Buseck, 2008; Li and Shao, 2009b; Geng et al., 2010; Gieré and Querol, 2010; Li and Shao, 2010; Ueda et al., 2011; Zhang et al., 2013; Li et al., 2014b], scanning transmission X-ray microscopy (STXM) with near-edge X-ray absorption fine structure spectroscopy [Takahama et al., 2010], and hygroscopic tandem differential mobility analyzer instruments [McMurry, 2000; Swietlicki et al., 2008; Anttila, 2010; Cheng et al., 2012]. In addition, the dependence of optical properties on the mixing state (coating thickness and coating materials) of black carbon (BC) aerosol has been investigated using the single-particle soot photometer [Shiraiwa et al., 2008; Oshima et al., 2009]. Until now, ATOFMS and TEM are the best techniques to determine chemical composition and mixing state of single particles. ATOFMS is an instrument that can reveal the mixing state of size-resolved single particles consisting of both refractory and nonrefractory species based on their mass spectrometry [Yang et al., 2009; Pratt and Prather, 2010; Zhang et al., 2013]. Likewise, TEM is the only instrument that can provide the mixing state of an individual particle based on chemical composition and morphology [Posfai and Buseck, 2010; Li et al., 2016]. Recently, individual particles analyzed by ATOFMS and scanning transmission X-ray microscopy (STXM) have enabled the calculation of the mixing state index (χ) [Healy et al., 2014; O'Brien et al., 2015]; however, the mixing state of an individual particle was not assessed. Compared to ATOFMS, TEM cannot analyze thousands of individual particles in a timely manner; it nonetheless clearly provides detailed information on the mixing structure of different aerosol species for individual particles. To overcome this shortcoming of TEM, some studies have classified particle types based on several hundred analyzed particles and summarized their characterization so that these analyzed data represent the collected sample [Adachi and Buseck, 2008; Deboudt et al., 2010; China et al., 2014; Li et al., 2014b, 2016]. Therefore, TEM remains one of the better methods to study the real mixing state of individual particles.

Evidence from laboratory, field measurements, and modeling studies shows that the aging processes of aerosol particles can convert them from external to internal mixtures at the population scale. At the scale of individual particles, different studies use different techniques to understand the mixing state of individual particles. They tend to have different concepts of what a "mixing state" actually means. For example, to understand optical properties of aerosol particles, individual aerosol particles composed of mixtures of different components (referred to as internally mixed particles) interact differently with light [Lang-Yona et al., 2010]. These studies do not consider internal mixing among nonabsorbing components, even though these mixtures could change the hygroscopic properties of these aerosol particles [Swietlicki et al., 2008]. In addition, and more fundamentally, the resolution of any technique determines its ability to identify mixing properties of individual particles [Posfai and Buseck, 2010; Li et al., 2016]. TEM, for example, is limited in its ability to identify different species in homogeneous particles that contain soluble organic matter, sulfate, and/or nitrate.

Several research groups study the chemical composition, morphology, and mixing state of individual particles using TEM [Buseck and Posfai, 1999; Hand et al., 2005; Adachi and Buseck, 2008; Li and Shao, 2009a; Gieré and Querol, 2010; Ueda et al., 2011; Zhu et al., 2013]. These studies classify particle types and describe the morphology and mixing state of individual particles, most often focused on several specific particle

species and on possible mixing mechanisms. To our knowledge, no study has systematically examined the mixing state of individual particles in various atmospheric environments and built conceptual models of how aerosol particles mix, two aspects of mixing state knowledge that would provide critical information for climate and aerosol-cloud-precipitation modeling. As a result, no consistent application of mixing rules has emerged from these different studies. To clarify this issue, we classified the particle types and summarized the mixing states of individual particles collected at urban, suburban, rural, clean background, and mountaintop sites and from the two different sources of biomass burning and coal combustion. The morphology, size, composition, and mixing state of thousands of particles were observed through TEM coupled with energy-dispersive X-ray spectrometry (TEM/EDS). In this paper, we focus on the mixing state of individual particles and will simply refer to it as mixing state for the remainder of the paper.

2. Experiments

2.1. Sampling Locations and Aerosol Sampling

We collected aerosol samples at different sampling sites, such as urban, suburban, rural, clean background, and mountaintop, as well as from two different sources of biomass burning and coal combustion. Sampling locations of an urban Beijing site, a suburban Xianghe site, a rural Yucheng site, a clean background Greater Khingan site, and a mountaintop Tai site are shown in Figure 1.

The urban site, located on the campus of the China University of Mining and Technology (39°59'N, 116°20'E) in the northwest area of Beijing, is surrounded by commercial buildings and residential apartments (Figure 1). The sampler was on the roof of a five-story building, 18 m above ground level. The sampling period was 1–3 June 2013 (Table 1).

The suburban site, located in suburban Xianghe (39°48'N, 116°57'E) about 50 km southeast of downtown Beijing and 85 km northwest of downtown Tianjin, is situated close to agricultural land, densely clustered residences, and some industries, and is 5 km west of Xianghe's town center (with a population of ~50,000; Figure 1). During the sampling period, the site experienced frequent mixed plumes from urban activities and industries during the daytime (Figure S1 in the supporting information) and was influenced by emissions from open barbecue cooking at night (1800–2400). Therefore, we selected daytime samples to avoid local anthropogenic sources. The sampling period was 1–10 June 2013 (Table 1).

The rural site is within the Yucheng Integrated Agricultural Experimental Station (36°57'N, 116°36'E) in Shandong Province (Table 1). The influence of local air pollutant emissions on the site is limited to agricultural activities (e.g., open agricultural biomass burning), although long-range transported pollutants are found in elevated concentrations in this area (Figure S1). For example, one regional haze episode formed on 2–3 June on the North China Plain [Sun *et al.*, 2016]: aerosol samples were collected during this haze episode. The sampling period was 1–10 June 2013 (Table 1).

Our clean background site is located in southeastern Greater Khingan. There is a small discarded airport surrounded by the forest, and no people live within 100 km (Figure 1). Natural sources and open biomass burning are the major sources of aerosol particles at this site. The sampling period was 25–27 September 2014 (Table 1).

A site near the top of Mount Tai (36°15'N, 117°06'E; 1534 m above sea level), which is the highest mountain located on the central North China Plain (Figure 1), represents long-range transported aerosol particles around the planetary boundary layer [Li *et al.*, 2011]. We collected aerosol samples in clouds under high relative humidity (RH). Three samples were collected on the two cloudy days of 22 July and 1 August 2014 (Table 1).

Biomass-burning samples were collected during open agricultural biomass burning in Linyi City, Shandong Province (Figure 1). Farmers burn the wheat biomass in agricultural fields in rural areas in eastern China in May and June of every year. We collected source samples about 5–15 m away from burning agricultural field to obtain fresh particles. The sampling was conducted on 10 June 2014 (Table 1).

Coal combustion samples were collected from emissions of a rural stove in winter 2015. The block coal is from Shanxi Province, which has the largest coal reserves in China. The source sample represents fresh aerosol particles from coal burning in northern China.

Aerosol particles were collected onto copper TEM grids coated with carbon film (carbon type B, 300-mesh copper; TianId Co., China) by a single-stage cascade impactor with a 0.5 mm diameter jet nozzle and an



Figure 1. Locations of five different sampling sites: urban Beijing, suburban Xianghe, rural Yucheng, clean background Greater Khingan, and Mount Tai sites, as well as two different sources: open agricultural biomass burning in Linyi and coal combustion in a rural stove (coal from Shanxi Province).

airflow rate of 1.0 L min^{-1} . This sampler has a collection efficiency close to 100% at $0.5 \mu\text{m}$ aerodynamic diameter for particles with a density of 2 g cm^{-3} [Marple *et al.*, 1993]. The sampler collects particles $>50 \text{ nm}$ with a different collection efficiency. Sampling times varied from 1 to 20 min, depending on particle loading estimated from visibility. After collection, each sample was placed in a sealed dry plastic tube and stored in a desiccator at 25°C and $20 \pm 3\% \text{ RH}$ to minimize exposure to ambient air before analysis.

2.2. TEM Analysis

Five aerosol samples from the urban site, 13 samples from the suburban site, 8 samples from the rural site, 3 samples from the clean background site, 3 samples from the cloudy days on the mountaintop site, 2 samples from biomass burning, and 2 samples from coal combustion were analyzed with a JEOL JEM-2100 TEM

Table 1. Sampling Information, Meteorological Conditions, and Main Sources During Sampling Periods

| Sampling Site | Sampling Date | T (°C) | RH (%) | WS (m/s) | Main Sources Around Location |
|---|---------------------------|--------|------------|----------|---|
| Urban (Beijing) | 1–3 June 2013 | 26–30 | 44–57% | 0.2–2.1 | Vehicle |
| Suburban (Xianghe) | 1–10 June 2013 | 18–28 | 15–80% | 0.1–1.5 | Industrial, biomass burning, and open cooking emissions |
| Rural (Yucheng) | 1–10 June 2013 | 16–28 | 32–90% | 0.2–5 | Biomass burning |
| Clean background (Greater Khingan) | 25–27 September 2014 | 10–25 | 18–50 | No data | Natural source and minor from biomass burning |
| Planetary boundary layer (Mountain Tai) | 22 July and 1 August 2014 | 18–22 | 100% cloud | 4–5 | Mixed pollutants from North China Plain |
| Open biomass burning (Linyi) | 10 June 2014 | - | - | - | Sample collection in burning plume of wheat |
| Coal combustion | 10 December 2015 | - | - | - | Shanxi block coal burning in rural stove |

operated at 200 kV. The distribution of aerosol particles on TEM grids was not uniform, with coarser particles impacting near the center and finer particles on the periphery. Therefore, to ensure that the analyzed particles were representative, five areas were chosen from the center and periphery of each grid. Every particle in the selected area was analyzed. Elemental composition was determined semiquantitatively using an energy-dispersive X-ray spectrometer (EDS) that can detect elements heavier than C. Copper (Cu) was excluded from the analyses, because the TEM grids are made of Cu. EDS spectra were collected for 15 s to determine the composition of individual aerosol particles. In these TEM analyses, water, semivolatile organics, and NH_4NO_3 were not quantified.

Because we can observe particle interiors through high-resolution TEM, we carefully check for the presence of different species (e.g., mineral, metal, fly ash, organics, and sulfate) within individual particles, noting any distinctive particle morphology, such as coatings, inclusions, and aggregations. We measured 3091 particles from urban and suburban, 964 particles from rural, 340 particles from clean background, 510 particles from mountaintop, 224 particles from biomass burning, and 81 particles from coal-combustion samples. For statistical analysis, the projected areas of individual particles were determined using iTEM software (Olympus soft imaging solutions GmbH, Germany), the conventional image analysis platform for electron microscopy.

2.3. Chemical Imaging of Individual Particles

Particle samples from Xianghe were analyzed using a CAMECA NanoSIMS 50 L at the Institute of Geology and Geophysics, Chinese Academy of Sciences. A $^{133}\text{Cs}^+$ primary beam current of 1–2 pA with a beam size of ~ 100 nm was used during the measurements. The scanning area of the primary beam ranged within a focal area of $30 \times 30 \mu\text{m}^2$. Secondary ions including $^{12}\text{C}^-$, $^{16}\text{O}^-$, $^{12}\text{C}^{14}\text{N}^-$, and $^{32}\text{S}^-$ were detected with electron multipliers in a multicollection mode. Because the substrate of our TEM grid was carbon, $^{12}\text{C}^{14}\text{N}^-$ was chosen to represent organic matter (OM) in individual particles. $^{32}\text{S}^-$ was used to infer the presence of sulfates. A similar procedure is described by Ghosal *et al.* [2014]. The NanoSIMS analysis can provide elemental mapping of particles with nanometer spatial resolution over a broad range of particle sizes. Recently, the NanoSIMS technique has been successfully applied to study aerosol particles [Harris *et al.*, 2012; Pöhlker *et al.*, 2012; Ghosal *et al.*, 2014].

3. Results and Discussion

3.1. Defining Externally and Internally Mixed Particles

Various single-particle analytical techniques have shown that aerosol compounds of individual particles are exceedingly complicated and that one particle could contain more than 10 different compounds [Buseck and Posfai, 1999; Li and Shao, 2009a; Moffet and Prather, 2009; Yang *et al.*, 2009; Posfai and Buseck, 2010; Ueda *et al.*, 2011; Healy *et al.*, 2014; Chi *et al.*, 2015]. Given this complexity, it is impossible to examine all of the various compounds in individual particles with a single analytical technique. The aerosol types shown in Figure 2 were examined by different analytical techniques; their combined results were used to discriminate externally and internally mixed particles [Li *et al.*, 2016].

Primary particles are directly emitted from natural or anthropogenic sources, such as mineral dust particles from deserts, soot and OM from incomplete combustion of fossil fuel, fly ash from coal combustion, sea salt from sea spray, and metals from heavy industries (Figure 2). Secondary particles arise through nucleation of trace acidic gases via various atmospheric reactions. ATOFMS reveals that secondary OM, sulfate, and/or nitrate are normally mixed well within the same individual secondary particle [Whiteaker *et al.*, 2002], but, and here is a critical caveat, nitrate cannot be identified by electron microscopy (e.g., Figure 2). These particle

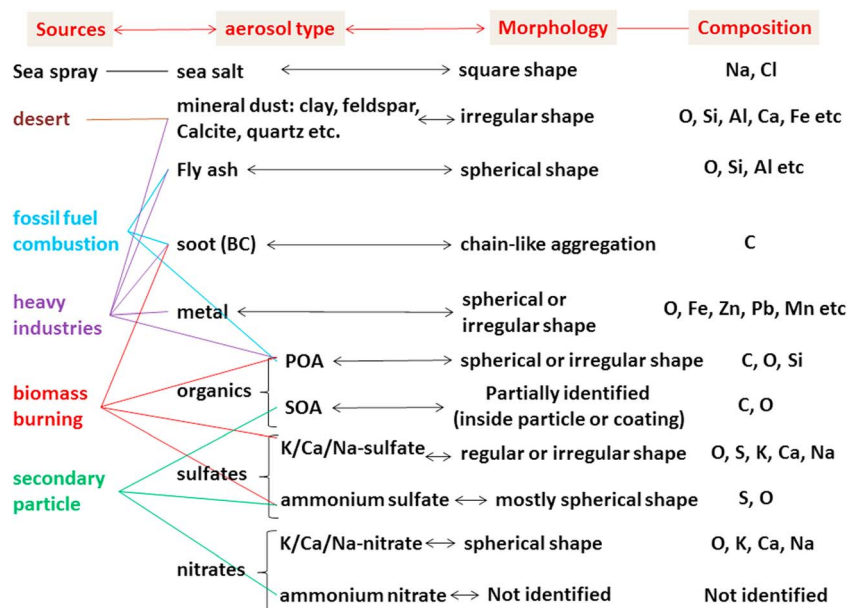


Figure 2. Different aerosol types based on TEM/EDS analysis and their possible sources.

classifications using TEM, SEM, and ATOFMS have been widely employed in various environmental settings, such as polluted urban air [Whiteaker et al., 2002; Adachi and Buseck, 2008; Li and Shao, 2009a; Moffet et al., 2010, 2013; Zhang et al., 2013], background air [Li et al., 2011; Niu et al., 2011; Ueda et al., 2011; Zhu et al., 2013; Li et al., 2014b], marine air [Chi et al., 2015], and in different source emissions [Hand et al., 2005; Laskin et al., 2005; Li and Shao, 2009b; Li et al., 2016]. Here we classified eight main types of aerosols: sea salt, mineral dust, fly ash, soot (BC), metal, organic matter (i.e., primary organic aerosols and secondary organic aerosols (SOAs)), sulfates (i.e., K/Ca/Na-sulfate or ammonium sulfate), and nitrates (i.e., K/Ca/Na-nitrate or ammonium nitrate; Figure 2).

A single particle that simultaneously contains two or more types of aerosol components is defined as an internally mixed particle. Otherwise, we defined it as an externally mixed particle (Figures 2 and 3a–3d). The externally mixed particles that are characterized as a single “type” does not mean they have a simple, uniform composition. For example, individual mineral dust particles would likely be a mixture of different minerals, such as clay, quartz, and feldspar. In this study, we propose that externally mixed particles retain their original properties from their initial sources, and any given type of externally mixed particle displays similar optical and/or hygroscopic properties. It should be noted that some trace secondary aerosol species that differ from the host particle cannot be detected by TEM/EDS [Li et al., 2016]. Here we assigned such particles to externally mixed particles, because trace aerosol species do not influence their physical and chemical properties of their host particles.

Although secondary particles look similar in the TEM images of different size regimes, they may display different optical and/or hygroscopic properties because of their different mass fractions of sulfate, OM, and/or nitrate [Li et al., 2016]. All secondary aerosol particles were assigned to internally mixed particles. Secondary aerosol species are likely homogeneously mixed in individual particles, so these are called “homogeneous-like mixtures” (Figure 3e). Here we propose that internally mixed particles generally contain two or more types of aerosol components (Figure 2) and that the different components of internally mixed particles will necessarily affect their atmospheric character, such as their hygroscopic and optical properties.

3.2. Classifying Internally Mixed Individual Particles

Based on the morphology and chemical composition of thousands of individual particles, we classify internally mixed particles into five structural classes: homogenous-like, core-shell, dumbbell, OM-coating, and dispersed-OM structures. The latter four classes are collectively referred to as “heterogeneous mixtures” in this study.

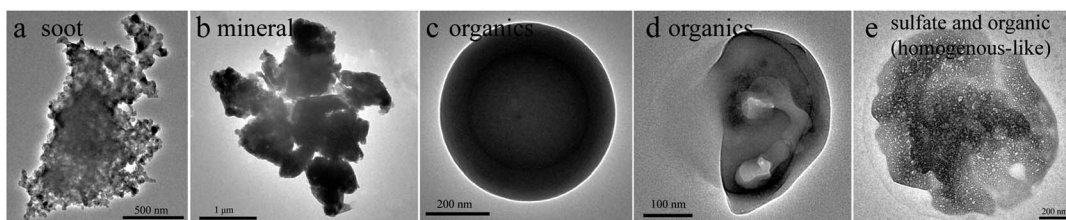


Figure 3. Four types of externally mixed particles and one typical homogeneous-like secondary particle: (a) soot, (b) mineral dust, (c) organics (tar ball), (d) organics, and (e) homogenous mixing of sulfate and organics.

3.2.1. Homogenous-Like Mixture

We define particles that solely consist of secondary aerosol components but have no specific shape in TEM images as “homogeneous mixtures” or “homogeneous-like” particles (Figure 3e). TEM observation shows that homogeneous-like particles display two typical morphologies, having smooth (Figures 4a, 4b, and 4f) and cracked surfaces (Figure 4e). Although TEM/EDS can only efficiently detect sulfur in secondary particles, these particles indeed are mixtures of sulfate, nitrate, and/or OM in the atmosphere, which can be identified using ATOFMS [Whiteaker *et al.*, 2002; Yang *et al.*, 2009]. However, TEM cannot identify all of the aerosol species in individual secondary particles. Individual particles of the homogeneous-like mixture type may display different hygroscopic properties, reflecting their different mass ratios of sulfate, nitrate, and OM (Table 2).

3.2.2. Core-Shell Structure

A core-shell structure is defined as primary particles coated with secondary aerosol materials. The common cores are mineral dust, salts (e.g., NaCl, KCl, and K_2SO_4) (Figure 4c), soot (Figures 4c, 4e, and 4g), organics (Figures 4b and 4g), metal (Figure 4a), or fly ash (Figures 4a and 4e).

Mineral dust core-shell structures in our study usually have a calcium/magnesium nitrate coating (Figure S2). These nitrate coatings are strongly correlated with the presence of alkaline mineral components (e.g., calcite and dolomite) [Laskin *et al.*, 2005; Li and Shao, 2009b]. Therefore, heterogeneous reactions of mineral particles and acidic gases lead to this type of internal mixing. Organic aerosols are directly emitted by fossil fuel combustion, biomass burning, and cooking but are also secondarily formed from gaseous volatile organic compounds (VOCs) in the atmosphere [Li *et al.*, 2016]. The primary organic particles normally have a spherical or irregular shape [Li and Shao, 2010]. These particles can be embedded within secondary aerosol species and form a core-shell structure, as shown in Figure 4b. Fine metal and fly ash particles with spherical shapes are mostly emitted from heavy industries and coal-fired power plants (Figure 2). These particles usually become coated with secondary aerosol species (e.g., Figures 4a, 4b, and 4g) during long-range transport.

Consisting of black carbon, soot particles are emitted from the incomplete combustion of biofuel, biomass burning, and fossil fuels (oil and coal; Figures 2 and 4c); they assume the form of chain-like aggregates of carbonaceous spheres with typical diameters from 10 to 100 nm (Figure 3a). Most soot particles are internally mixed with secondary aerosol species or K-rich particles. Such a mixture of soot and K-rich particles could be directly emitted from biomass burning (Figure 4c). The more typical mixture of soot and secondary aerosol species, however, probably forms through condensation and coagulation in the atmosphere [Jacobson, 2002; Shiraiwa *et al.*, 2008]. The shapes of soot particles vary with different sources and atmospheric aging; their morphology and size also are modified during atmospheric transport [Zhang *et al.*, 2008; Adachi *et al.*, 2010; Niu *et al.*, 2011; China *et al.*, 2013]. Therefore, internally mixed soot particles display complicated mixing structures (Figure 4e). Soot particles are frequently partially or entirely coated with secondary aerosol species (Figures 4c, 4e, and 4g) that form core-shell structures. The core of soot and shell of secondary aerosol species have been found in various locations [Adachi and Buseck, 2008; Li and Shao, 2009a; Niu *et al.*, 2011; Ueda *et al.*, 2011; Cheng *et al.*, 2012]. The shell of secondary aerosols not only can enhance optical absorption of the soot core but also increases the hygroscopicity of the soot particle so that it can act as a cloud condensation nucleus [Jacobson, 2001; McFiggans *et al.*, 2006; Adachi *et al.*, 2010; Bond *et al.*, 2013].

3.2.3. Dumbbell Structure

A dumbbell structure results from two or more particles of different types adhering to each other. For example, a small number of mineral particles contain secondary gypsum attached to aluminosilicate particles. This type of mixture results in a “dumbbell structure” (Figure 4f). When mineral dust, soot, and organic particles are combined in this way with hydrophilic secondary aerosol species (e.g., sulfate, nitrate, and OM),

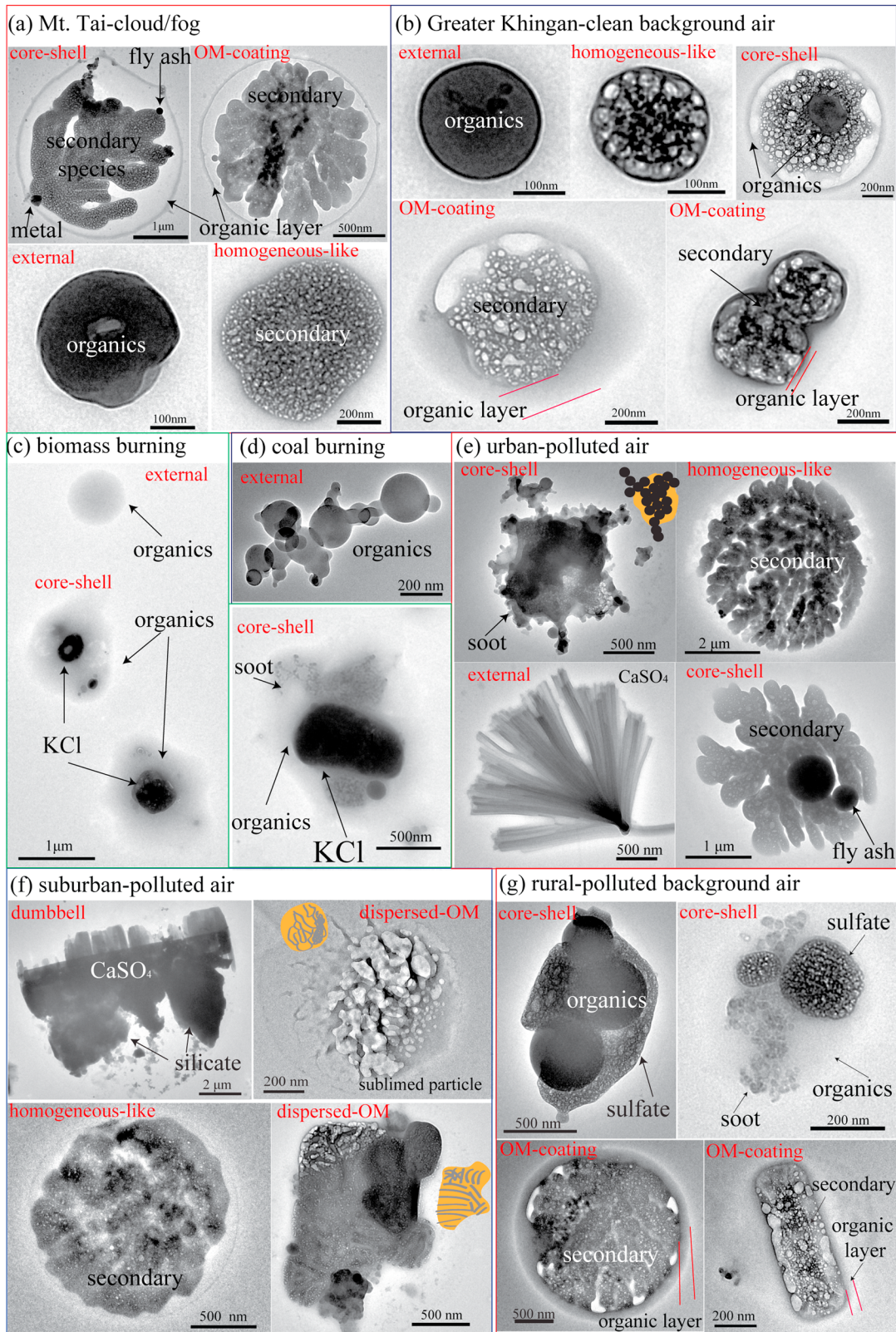


Figure 4. The major mixing structures of individual particles at different sampling sites. (a) Particles collected in cloud on top of Mount Tai. (b) Particles collected at a clean background Greater Khingan site. (c) Particles collected at an open agricultural biomass-burning site. (d) Particles collected from coal burning in a rural stove. (e) Particles collected at an urban site. (f) Particles collected at a suburban site. (g) Particles collected at a rural site (polluted background site).

Table 2. Summarizing Conceptual Model and Optical and Hygroscopic Properties Among Different Mixing Structures

| Mixing State | Mixing Structure | Conceptual Model | Aerosol Species | Direct Optical | Hygroscopic |
|------------------------|---------------------------|--|---|----------------|-------------|
| Internal | Homogenous-like structure | | Secondary inorganic aerosols (SIAs) and/or secondary organics | a | b |
| | Core-shell | | Soot core-SIA shell/organic shell | c | c |
| | | | Mineral core-SIA shell/nitrate shell | b | c |
| | Dumbbell | | Metal core-SIA shell | a | b |
| | | | Fly ash core-SIA shell | a | b |
| | | | OM and SIA | b | b |
| | OM coating | | Soot, SIA, and OM | a | b |
| Mineral and SIA | | | a | b | |
| Dispersed OM structure | | OM and SIA | a | b | |
| | | OM coating on SIA | b | b | |
| External | | Fly ash, mineral, and metal primary OM | a | a | |
| | | Soot | a | a | |

^aNo influence.

^bInfluenced.

^cHighly influenced.

their hygroscopicity may increase. The dumbbell structures might change the optical properties of either of the two constituent particles [Fuller *et al.*, 1999], particularly in the case of soot and secondary particles (Table 2), but these changes would likely be small.

3.2.4. OM-Coating Structure

An OM-coating structure is defined as a secondary inorganic particle coated by OM (Figure 4). The phase separation of OM and sulfate likely undergoes liquid-liquid phase separation in the air [You *et al.*, 2012]. The ion intensity threshold map of individual particles analyzed by the NanoSIMS in Figure 5 shows organic matter (CN⁻) clearly coating sulfate particles. A similar mixing structure was observed in individual particles collected in Mexico City using a NanoSIMS [Ghosal *et al.*, 2014]; this unique morphology was called “OM-coating structure.” The morphology of OM-coating particles is similar to core-shell structure, but OM-coating structure may change following OM aging process in the atmosphere. Moreover, the OM-coating structure can transform into a homogeneous-like mixture under higher RH. OM coatings on individual particles can change a host particle’s early hygroscopic properties [Semeniuk *et al.*, 2007; Li *et al.*, 2014a]. If the OM is brown carbon, then the OM coating will probably affect the optical properties of individual particles.

3.2.5. Dispersed-OM Structure

A dispersed-OM structure is defined as OM skeletons mixed with sulfates. The morphology of dispersed-OM particles clearly display an uneven surface, and OM skeletons are grey color, as in Figure 4f. When secondary inorganic species were sublimed under a strong electron beam, we could clearly observe the resulting void spaces among OM skeletons (Figure 4f). The sublimed particles mainly consisted of C, with lesser amounts of O and Si. The ion intensity threshold map of individual particles in Figure 5 shows that organic matter (CN⁻) was mixed within sulfate (S⁻) particles. Our results suggest that these skeletons within secondary particles mainly consist of OM (Figure 4f). In addition, some studies have found that secondary sulfate particles collected in upper atmospheric layers contain a “framework” of carbonaceous matter [Kojima *et al.*, 2005; Nguyen *et al.*, 2008]. The dispersed-OM structure is different from the common cracked particles in the atmosphere (e.g., Figure 4e), because these do not contain OM skeletons. We suspect that the cracked particles could form during recrystallization of aerosol components on the substrate or as a result of some semivolatile aerosol species evaporate during efflorescence. A dispersed-OM structure indicates that the OM is inhomogeneously dispersed within a particle consisting of inorganic secondary aerosol species (e.g., sulfates and nitrates). The secondary inorganic species likely change the hygroscopic properties of the OM (Table 2).

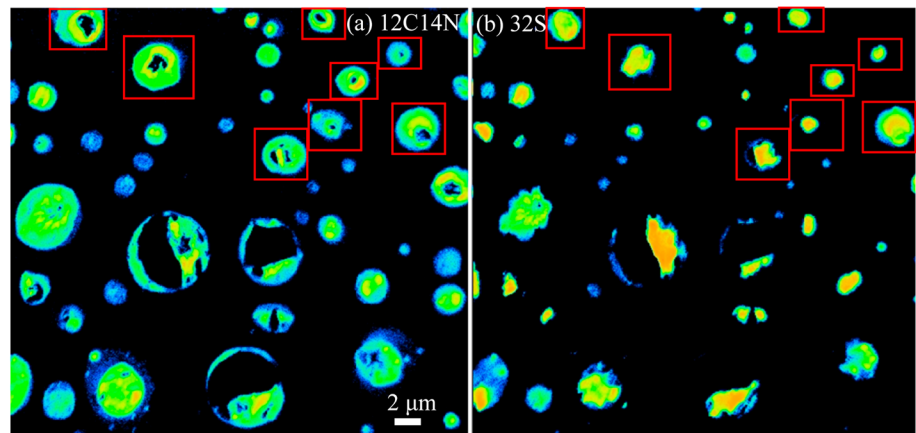


Figure 5. NanoSIMS intensity threshold maps of (a) $^{12}\text{C}^{14}\text{N}^-$ and (b) $^{32}\text{S}^-$ of individual particles at the Xianghe site. The red rectangles indicate the OM coating; others have dispersed-OM or homogeneous-like structure.

3.3. Quantifying the Fraction of Particles with Different Mixing Structures

Figure 6 displays the percentages of different mixing structures in internally mixed particles and externally mixed particles at different sampling sites. Externally mixed and homogenous mixture particles were mainly observed in fine particles (less than $1\ \mu\text{m}$) at all five sampling sites. We did not observe secondary

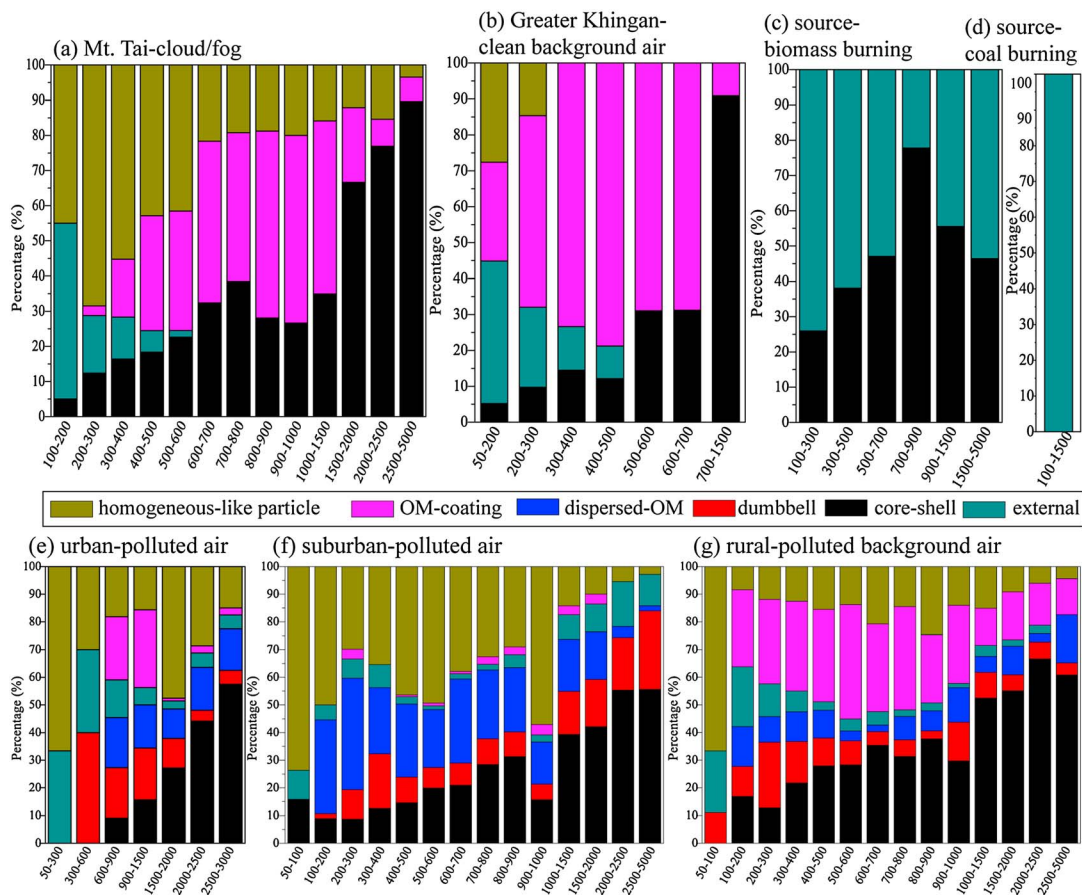


Figure 6. Size distributions of different mixing structures of individual particles at different sampling sites. (a) The 510 analyzed particles collected in cloud on top of Mount Tai. (b) The 340 analyzed particles collected at a clean background Greater Khingan site. (c) The 224 analyzed particles collected at an open agricultural biomass-burning site. (d) The 81 analyzed particles collected from coal burning in rural stove. (e) The 287 analyzed particles collected at an urban site. (f) The 2804 analyzed particles collected at an urban/suburban site. (g) The 964 analyzed particles collected at a rural site (polluted background site). OM denotes organic matter.

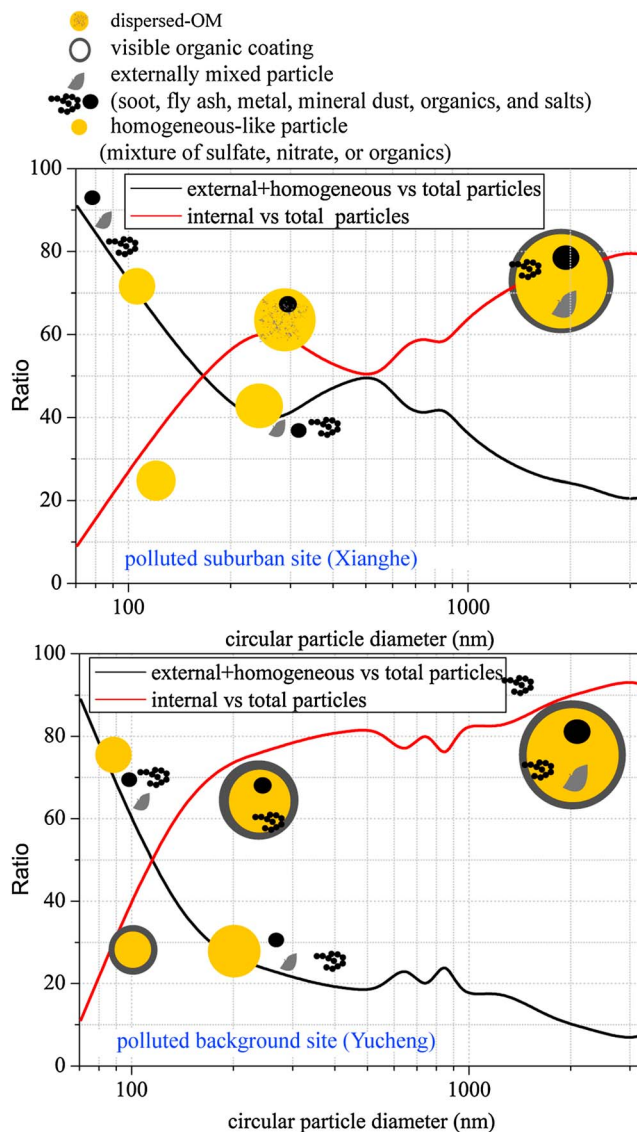


Figure 7. Heterogeneously internally mixed particles (internal) and external mixed particles (external) plus homogeneous-like (homogeneous) particles versus total analyzed particles by particle number at polluted suburban sites and a rural site during the same sampling period. These data are from Figure 6. The ratio of external to total particles decreases; the ratio of internal to total particles increases with an increase in particle size. Internally mixed particles consist of core-shell, OM coating, dispersed OM, and dumbbell. OM denotes organic matter.

secondary particles. *You et al.* [2012] showed that particles display an OM-coating structure in lower RH through liquid-liquid phase separations and that they become well-mixed liquid particles after separation at higher RH. Such liquid-liquid phase separation occurred in internally mixed particles containing secondary sulfates and SOA ($O:C < 0.8$) [*Mikhailov et al.*, 2009; *You et al.*, 2012].

Figures 6e–6g show that the percentage of dispersed-OM particles is much higher at urban/suburban sites than at rural sites. At the suburban sampling site, we found dispersed-OM structure in many secondary particles rather than forming a clear OM coating (Figure 4f). It is not entirely clear why the internally mixed particles of OM and secondary inorganic aerosols form a dispersed-OM structure instead of an OM-coating structure at urban and suburban sites; one possibility may be the extent of oxidation of

homogeneous-like mixture particles from biomass-burning or coal-burning emissions but found many externally mixed particles (Figures 4c, 4d, 6c, and 6d).

The core-shell structure is dominant in coarse particles ($>1 \mu\text{m}$) in clean and polluted air. TEM observations show that soot (Figures 4c, 4e, and 4g) and OM particles (Figures 4b and 4g) were the most common materials comprising the cores that are coated with sulfate and organic shells in urban, rural, and clean background air. Although we found abundant core-shell structure particles in all the size ranges from biomass-burning emissions (Figure 6c), the percentages of core-shell particles generally increased with increasing particle size in clean and polluted air (Figures 6a, 6b, and 6e–6g).

Considering the OM-coating structures at different sampling sites, we found that OM coating mainly occurred in the aged air masses (Figures 6a, 6b, and 6g), rather than fresh air masses from either biomass-burning/coal-combustion emission sources (Figures 6c and 6d), or the polluted urban/suburban atmospheres (Figures 6e and 6f). This result is consistent with the previous studies. For example, studies reporting OM-coating structure in particles have generally been carried out in background areas, such as Dongying, Shandong [*Li et al.*, 2014b], in the outflow from Mexico City [*Moffet et al.*, 2010], and in the Central Valley of California [*Moffet et al.*, 2013]. These investigators suggest that condensation of SOA produces an organic coating on

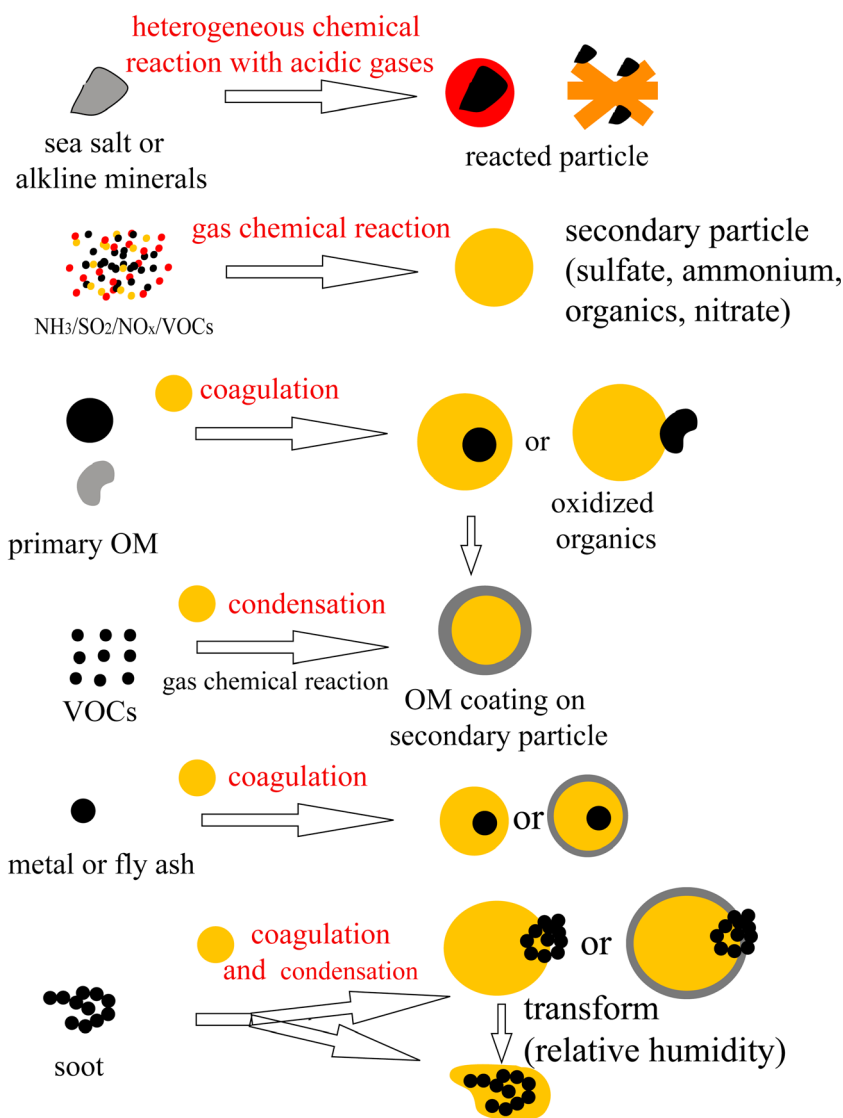


Figure 8. Schematic of mixing structures of different particle types based on TEM observation. These mixing structures only represent atmospheric solid particles.

OM [Kojima *et al.*, 2005; Nguyen *et al.*, 2008]. To our knowledge, dispersed-OM structures of individual particles are not commonly reported in field experiments.

TEM shows that fine particles, such as metal, fly ash, and soot, tend to be internally mixed with coarse secondary particles. Figure 7 compares the ratio of heterogeneous internally mixed particles versus total particles at polluted suburban and rural sites during the same sampling period. We found this ratio increases with particle size, while the ratio of externally mixed plus homogeneous-like particles versus total particles decreases. This result is consistent with an investigation by Bauer *et al.* [2013] using the ATOFMS. This phenomenon could arise because secondary sulfate, nitrate, and organic materials are the major inducers of internal mixing in the atmosphere. Two general observations support this statement. The first is that the highest number and mass concentration of secondary aerosols are mainly formed through new particle formation processes involving acidic gases and heterogeneous chemical reactions on primary particles [McMurry, 2000; Harris *et al.*, 2012; Kulmala *et al.*, 2013; Li *et al.*, 2014b; O'Brien *et al.*, 2015]. The second is that the phase of secondary aerosols changes from solid to liquid following a RH increase; hence, the liquid particles tend to stick to a solid phase through particle coagulation [Jacobson, 2002]. Indeed, we found that many droplets collected in cloudy conditions on Mount Tai contained insoluble cores such as soot, fly ash,

and metal (e.g., Figures 4a and 6a). It should be noted that internally mixed coarse particles with complex structures developed their precise morphology dependent on a specific source type and on the atmospheric RH.

3.4. Developing a Conceptual Framework and Understanding Its Atmospheric Implications

Based on the results and discussion above, we propose a framework for the formation of different mixing structures (Figure 8). TEM observations show that secondary aerosol species are important aerosol components that mix with metal, fly ash, OM, and soot particles (Figure 4). Secondary particles, including ammonium, OM, sulfate, and nitrate, mainly nucleate from acidic gases (e.g., NO_x and SO_2), although some volatile organic compounds (VOCs) also participate in their formation [Whiteaker et al., 2002; Kulmala et al., 2013]. These micro-scale atmospheric processes convert externally mixed particles into internally mixed particles. Once externally mixed particles are transformed into internally mixed particles, they cannot revert to their initial state, except when semivolatile aerosol material is involved (e.g., NH_4NO_3 and some OM). However, different mixing structures of internally mixed particles can be altered by particle aging processes, as shown in Figure 8.

Based on the results from different sampling sites, dispersed-OM and dumbbell structures are not common mixing structures (Figure 6) and tend to transform into OM-coating and core-shell structures (Figure 8). We conclude that OM-coating and core-shell structures are important indicators of particle aging in clean and polluted air (Figure 6), except when close to the specific emission sources [Semeniuk et al., 2015].

Bauer et al. [2013] suggested that the knowledge of realistic mixing structures of individual particles is necessary to explain their hygroscopicity, cloud condensation nucleus activity, and optical properties in field measurements and modeling simulations. The secondary aerosol species that form particle coatings can change the hygroscopic properties of core particles (e.g., spherical OM, fly ash, metal, mineral, and soot) from hydrophobic to hydrophilic (Table 2). The shell can also enhance light absorption on soot cores (black carbon) [Jacobson, 2001]. It should be noted that secondary aerosol species can also change the size distribution of cores (Figure S3). For example, when evaluating the size of metal particles through ATOFMS and a multistage sampler, it is necessary to consider the influences of core-shell or dumbbell structures. Moreover, metal particles that are internally mixed with acidic secondary aerosol species can release toxic metal ions in multiphase chemical reactions during their long-range transport and further influence human health [Li et al., 2013]. Knowing size differences between externally and internally mixed metal particles and their mixing structures can lead to a more accurate evaluation of their influences on ecology and human health.

To complicate matters further, the mixing of OM and secondary aerosol species occurs differently in different locations. The OM coating of individual particles has most often been reported in background areas [Moffet et al., 2010, 2013; Li et al., 2014b]; however, studies of dispersed-OM structures of individual particles are uncommon, possibly in part because of the technical difficulty involved in their detection. These different mixing structures would induce different hygroscopic and optical properties of individual particles (Table 2). SOA coating to particles can significantly affect their deliquescence RH and optical properties [Zelenyuk et al., 2008; Mikhailov et al., 2009; Lang-Yona et al., 2010; Takahama et al., 2010; Robinson et al., 2013]. In addition, SOA coatings can change heterogeneous reactions on particle surfaces [You et al., 2012] and inhibit water evaporation from individual secondary particles [Davies et al., 2013]. More importantly, the solid surface-confined chemistry and kinetic limitations involved in equilibrium partitioning between the gas and solid phases can be impeded by viscous organic coatings [Shiraiwa et al., 2011].

Although the mixing structures of individual particles are complicated in the atmosphere, we can summarize the mixing rules for different particle types (Figure 8). Conceptualizing the mixing structure of individual internally mixed particles in this way help to evaluate their optical and hygroscopic properties and to understand possible heterogeneous reactions on particle surfaces. Therefore, OM-coating, core-shell, and homogeneous-like particles in clean and polluted air should be classified as distinct types and, insofar as possible, incorporated into regional climate models, aerosol-cloud-precipitation models, and experimental and field measurements.

References

- Adachi, K., and P. R. Buseck (2008), Internally mixed soot, sulfates, and organic matter in aerosol particles from Mexico City, *Atmos. Chem. Phys.*, 8(21), 6469–6481.
- Adachi, K., S. H. Chung, and P. R. Buseck (2010), Shapes of soot aerosol particles and implications for their effects on climate, *J. Geophys. Res.*, 115, D15206, doi:10.1029/2009JD012868.

Acknowledgments

We appreciate Peter Hyde's comments and proofreading. This work was funded by grants from the National Key Project of MOST (JFYS2016ZY01002213); National Natural Science Foundation of China (41575116 and 41622504); Strategic Priority Research Program (B) of the Chinese Academy of Sciences (XDB05020500); Shandong Provincial Science Fund for Distinguished Young Scholars, China (JQ201413); and Programs of Shandong University (2014QY001/2015WLJH37). All images and the related additional data are available from W.J.L. (e-mail: liweijun.atmos@gmail.com).

- Anttila, T. (2010), Sensitivity of cloud droplet formation to the numerical treatment of the particle mixing state, *J. Geophys. Res.*, *115*, D21205, doi:10.1029/2010JD013995.
- Bauer, S. E., A. Ault, and K. A. Prather (2013), Evaluation of aerosol mixing state classes in the GISS modelE-MATRIX climate model using single-particle mass spectrometry measurements, *J. Geophys. Res. Atmos.*, *118*, 9834–9844, doi:10.1002/jgrd.50700.
- Bond, T. C., et al. (2013), Bounding the role of black carbon in the climate system: A scientific assessment, *J. Geophys. Res. Atmos.*, *118*, 5380–5552, doi:10.1002/jgrd.50171.
- Buseck, P. R., and M. Posfai (1999), Airborne minerals and related aerosol particles: Effects on climate and the environment, *Proc. Natl. Acad. Sci. U.S.A.*, *96*(7), 3372–3379.
- Cheng, Y. F., et al. (2012), Size-resolved measurement of the mixing state of soot in the megacity Beijing, China: Diurnal cycle, aging and parameterization, *Atmos. Chem. Phys.*, *12*(10), 4477–4491.
- Chi, J. W., et al. (2015), Sea salt aerosols as a reactive surface for inorganic and organic acidic gases in the Arctic troposphere, *Atmos. Chem. Phys.*, *15*(19), 11,341–11,353.
- China, S., C. Mazzoleni, K. Gorkowski, A. C. Aiken, and M. K. Dubey (2013), Morphology and mixing state of individual freshly emitted wildfire carbonaceous particles, *Nat. Commun.*, *4*, doi:10.1038/ncomms3122.
- China, S., N. Salvadori, and C. Mazzoleni (2014), Effect of traffic and driving characteristics on morphology of atmospheric soot particles at freeway on-ramps, *Environ. Sci. Technol.*, *48*(6), 3128–3135.
- Dall'Osto, M., R. M. Harrison, E. J. Highwood, C. O'Dowd, D. Ceburnis, X. Querol, and E. P. Achterberg (2010), Variation of the mixing state of Saharan dust particles with atmospheric transport, *Atmos. Environ.*, *44*(26), 3135–3146.
- Davies, J. F., R. E. H. Miles, A. E. Haddrell, and J. P. Reid (2013), Influence of organic films on the evaporation and condensation of water in aerosol, *Proc. Natl. Acad. Sci. U.S.A.*, *110*(22), 8807–8812.
- Deboudt, K., P. Flament, M. Choel, A. Gloter, S. Sobanska, and C. Colliex (2010), Mixing state of aerosols and direct observation of carbonaceous and marine coatings on African dust by individual particle analysis, *J. Geophys. Res.*, *115*, D24207, doi:10.1029/2010JD013921.
- Fuller, K. A., W. C. Malm, and S. M. Kreidenweis (1999), Effects of mixing on extinction by carbonaceous particles, *J. Geophys. Res.*, *104*, 15,941–15,954, doi:10.1029/1998JD100069.
- Fuzzi, S., et al. (2006), Critical assessment of the current state of scientific knowledge, terminology, and research needs concerning the role of organic aerosols in the atmosphere, climate, and global change, *Atmos. Chem. Phys.*, *6*(7), 2017–2038.
- Geng, H., S. Kang, H.-J. Jung, M. Choel, H. Kim, and C.-U. Ro (2010), Characterization of individual submicrometer aerosol particles collected in Incheon, Korea, by quantitative transmission electron microscopy energy-dispersive X-ray spectrometry, *J. Geophys. Res.*, *115*, D15306, doi:10.1029/2009JD013486.
- Ghosal, S., P. K. Weber, and A. Laskin (2014), Spatially resolved chemical imaging of individual atmospheric particles using nanoscale imaging mass spectrometry: Insight into particle origin and chemistry, *Anal. Methods*, *6*(8), 2444–2451.
- Gibson, E. R., P. K. Hudson, and V. H. Grassian (2006), Aerosol chemistry and climate: Laboratory studies of the carbonate component of mineral dust and its reaction products, *Geophys. Res. Lett.*, *33*, L13811, doi:10.1029/2006GL026386.
- Gieré, R., and X. Querol (2010), Solid particulate matter in the atmosphere, *ELEMENTS*, *6*(4), 215–222.
- Hand, J. L., et al. (2005), Optical, physical, and chemical properties of tar balls observed during the Yosemite Aerosol Characterization Study, *J. Geophys. Res.*, *110*, D21210, doi:10.1029/2004JD005728.
- Harris, E., B. Sinha, S. Foley, J. N. Crowley, S. Borrmann, and P. Hoppe (2012), Sulfur isotope fractionation during heterogeneous oxidation of SO₂ on mineral dust, *Atmos. Chem. Phys.*, *12*(11), 4867–4884.
- Healy, R. M., et al. (2014), Single particle diversity and mixing state measurements, *Atmos. Chem. Phys.*, *14*(12), 6289–6299.
- Jacobson, M. Z. (2001), Strong radiative heating due to the mixing state of black carbon in atmospheric aerosols, *Nature*, *409*(6821), 695–697.
- Jacobson, M. Z. (2002), Analysis of aerosol interactions with numerical techniques for solving coagulation, nucleation, condensation, dissolution, and reversible chemistry among multiple size distributions, *J. Geophys. Res.*, *107*(D19), 4366, doi:10.1029/2001JD002044.
- Kojima, T., P. R. Buseck, and J. M. Reeves (2005), Aerosol particles from tropical convective systems: 2. Cloud bases, *J. Geophys. Res.*, *110*, D09203, doi:10.1029/2004JD005173.
- Kulmala, M., et al. (2013), Direct observations of atmospheric aerosol nucleation, *Science*, *339*(6122), 943–946.
- Lang-Yona, N., A. Abo-Riziq, C. Erlick, E. Segre, M. Trainic, and Y. Rudich (2010), Interaction of internally mixed aerosols with light, *Phys. Chem. Chem. Phys.*, *12*(1), 21–31.
- Laskin, A., M. J. Iedema, A. Ichkovich, E. R. Graber, I. Taraniuk, and Y. Rudich (2005), Direct observation of completely processed calcium carbonate dust particles, *Faraday Discuss.*, *130*, 453–468.
- Lesins, G., P. Chylek, and U. Lohmann (2002), A study of internal and external mixing scenarios and its effect on aerosol optical properties and direct radiative forcing, *J. Geophys. Res.*, *107*(D10), 4094, doi:10.1029/2001JD000973.
- Li, W. J., and L. Y. Shao (2009a), Transmission electron microscopy study of aerosol particles from the brown hazes in northern China, *J. Geophys. Res.*, *114*, D05202, doi:10.1029/2008JD011285.
- Li, W. J., and L. Y. Shao (2009b), Observation of nitrate coatings on atmospheric mineral dust particles, *Atmos. Chem. Phys.*, *9*(6), 1863–1871.
- Li, W. J., and L. Y. Shao (2010), Mixing and water-soluble characteristics of particulate organic compounds in individual urban aerosol particles, *J. Geophys. Res.*, *115*, D02301, doi:10.1029/2009JD012575.
- Li, W. J., D. Z. Zhang, L. Y. Shao, S. Z. Zhou, and W. X. Wang (2011), Individual particle analysis of aerosols collected under haze and non-haze conditions at a high-elevation mountain site in the North China Plain, *Atmos. Chem. Phys.*, *11*(22), 11,733–11,744.
- Li, W., T. Wang, S. Zhou, S. Lee, Y. Huang, Y. Gao, and W. Wang (2013), Microscopic observation of metal-containing particles from Chinese continental outflow observed from a non-industrial site, *Environ. Sci. Technol.*, *47*(16), 9124–9131.
- Li, W., et al. (2014a), Composition and hygroscopicity of aerosol particles at Mt. Lu in South China: Implications for acid precipitation, *Atmos. Environ.*, *94*, 626–636.
- Li, W., et al. (2014b), Mixing state and hygroscopicity of dust and haze particles before leaving Asian continent, *J. Geophys. Res. Solid Earth*, *119*, 1044–1059, doi:10.1002/2013JB010599.
- Li, W., L. Shao, D. Zhang, C.-U. Ro, M. Hu, X. Bi, H. Geng, A. Matsuki, H. Niu, and J. Chen (2016), A review of single aerosol particle studies in the atmosphere of East Asia: Morphology, mixing state, source, and heterogeneous reactions, *J. Clean. Prod.*, *112*(Part 2), 1330–1349.
- Liu, Y., J. P. Cain, H. Wang, and A. Laskin (2007), Kinetic study of heterogeneous reaction of deliquesced NaCl particles with gaseous HNO₃ using particle-on-substrate stagnation flow reactor approach, *J. Phys. Chem. A*, *111*, 10,026–10,043.
- Marple, V. A., K. L. Rubow, and B. A. Olson (1993), Inertial, gravitational, centrifugal, and thermal collection techniques, in *Aerosol Measurement*, edited by K. Willike and P. A. Baron, pp. 206–233, Van Nostrand Reinhold, New York.
- McFiggans, G., et al. (2006), The effect of physical and chemical aerosol properties on warm cloud droplet activation, *Atmos. Chem. Phys.*, *6*(9), 2593–2649.

- McMurry, P. H. (2000), A review of atmospheric aerosol measurements, *Atmos. Environ.*, *34*(12–14), 1959–1999.
- Mikhailov, E., S. Vlasenko, S. T. Martin, T. Koop, and U. Poschl (2009), Amorphous and crystalline aerosol particles interacting with water vapor: Conceptual framework and experimental evidence for restructuring, phase transitions and kinetic limitations, *Atmos. Chem. Phys.*, *9*(24), 9491–9522.
- Moffet, R. C., and K. A. Prather (2009), In-situ measurements of the mixing state and optical properties of soot with implications for radiative forcing estimates, *Proc. Natl. Acad. Sci. U.S.A.*, *106*(29), 11,872–11,877.
- Moffet, R. C., et al. (2010), Microscopic characterization of carbonaceous aerosol particle aging in the outflow from Mexico City, *Atmos. Chem. Phys.*, *10*(3), 961–976.
- Moffet, R. C., T. C. Rödel, S. T. Kelly, X. Y. Yu, G. T. Carroll, J. Fast, R. A. Zaveri, A. Laskin, and M. K. Gilles (2013), Spectro-microscopic measurements of carbonaceous aerosol aging in central California, *Atmos. Chem. Phys.*, *13*(20), 10,445–10,459.
- Nguyen, H. N., et al. (2008), Chemical composition and morphology of individual aerosol particles from a CARIBIC flight at 10 km altitude between 50°N and 30°S, *J. Geophys. Res.*, *113*, D23209, doi:10.1029/2008JD009956.
- Niu, H., L. Shao, and D. Zhang (2011), Aged status of soot particles during the passage of a weak cyclone in Beijing, *Atmos. Environ.*, *45*(16), 2699–2703.
- O'Brien, R. E., et al. (2015), Chemical imaging of ambient aerosol particles: Observational constraints on mixing state parameterization, *J. Geophys. Res. Atmos.*, *120*, 9591–9605, doi:10.1002/2015JD023480.
- Oshima, N., M. Koike, Y. Zhang, and Y. Kondo (2009), Aging of black carbon in outflow from anthropogenic sources using a mixing state resolved model: 2. Aerosol optical properties and cloud condensation nuclei activities, *J. Geophys. Res.*, *114*, D06210, doi:10.1029/2008JD010680.
- Pöhlker, C., et al. (2012), Biogenic potassium salt particles as seeds for secondary organic aerosol in the Amazon, *Science*, *337*(6098), 1075–1078.
- Posfai, M., and P. R. Buseck (2010), Nature and climate effects of individual tropospheric aerosol particles, *Annu. Rev. Earth Planet. Sci.*, *38*(1), 17–43.
- Pratt, K. A., and K. A. Prather (2010), Aircraft measurements of vertical profiles of aerosol mixing states, *J. Geophys. Res.*, *115*, D11305, doi:10.1029/2009JD013150.
- Riemer, N., and M. West (2013), Quantifying aerosol mixing state with entropy and diversity measures, *Atmos. Chem. Phys.*, *13*(22), 11,423–11,439.
- Robinson, C. B., G. P. Schill, K. J. Zarzana, and M. A. Tolbert (2013), Impact of organic coating on optical growth of ammonium sulfate particles, *Environ. Sci. Technol.*, *47*(23), 13,339–13,346.
- Semeniuk, T. A., M. E. Wise, S. T. Martin, L. M. Russell, and P. R. Buseck (2007), Water uptake characteristics of individual atmospheric particles having coatings, *Atmos. Environ.*, *41*(29), 6225–6235.
- Semeniuk, T. A., R. Bruintjes, V. Salazar, D. Breed, T. Jensen, and P. R. Buseck (2015), Processing of aerosol particles within the Habshan pollution plume, *J. Geophys. Res. Atmos.*, *120*, 1996–2012, doi:10.1002/2014JD022279.
- Shiraiwa, M., Y. Kondo, N. Moteki, N. Takegawa, L. K. Sahu, A. Takami, S. Hatakeyama, S. Yonemura, and D. R. Blake (2008), Radiative impact of mixing state of black carbon aerosol in Asian outflow, *J. Geophys. Res.*, *113*, D24210, doi:10.1029/2008JD010546.
- Shiraiwa, M., M. Ammann, T. Koop, and U. Poschl (2011), Gas uptake and chemical aging of semisolid organic aerosol particles, *Proc. Natl. Acad. Sci. U.S.A.*, *108*(27), 11,003–11,008.
- Sun, Y., et al. (2016), Aerosol characterization over the North China Plain: Haze life cycle and biomass burning impacts in summer, *J. Geophys. Res. Atmos.*, *121*, 2508–2521, doi:10.1002/2015JD024261.
- Swietlicki, E., et al. (2008), Hygroscopic properties of submicrometer atmospheric aerosol particles measured with H-TDMA instruments in various environments—A review, *Tellus B*, *60*(3), 432–469.
- Takahama, S., S. Liu, and L. M. Russell (2010), Coatings and clusters of carboxylic acids in carbon-containing atmospheric particles from spectromicroscopy and their implications for cloud-nucleating and optical properties, *J. Geophys. Res.*, *115*, D01202, doi:10.1029/2009JD012622.
- Ueda, S., K. Osada, and A. Takami (2011), Morphological features of soot-containing particles internally mixed with water-soluble materials in continental outflow observed at Cape Hedo, Okinawa, Japan, *J. Geophys. Res.*, *116*, D17207, doi:10.1029/2010JD015565.
- Whiteaker, J. R., D. T. Suess, and K. A. Prather (2002), Effects of meteorological conditions on aerosol composition and mixing state in Bakersfield, CA, *Environ. Sci. Technol.*, *36*(11), 2345–2353.
- Yang, F., H. Chen, X. N. Wang, X. Yang, J. F. Du, and J. M. Chen (2009), Single particle mass spectrometry of oxalic acid in ambient aerosols in Shanghai: Mixing state and formation mechanism, *Atmos. Environ.*, *43*(25), 3876–3882.
- You, Y., et al. (2012), Images reveal that atmospheric particles can undergo liquid–liquid phase separations, *Proc. Natl. Acad. Sci. U.S.A.*, *109*(33), 13,188–13,193.
- Zelenyuk, A., J. Yang, C. Song, R. A. Zaveri, and D. Imre (2008), “Depth-profiling” and quantitative characterization of the size, composition, shape, density, and morphology of fine particles with SPLAT, a single-particle mass spectrometer, *J. Phys. Chem. A*, *112*(4), 669–677.
- Zhang, G., X. Bi, L. Li, L. Y. Chan, M. Li, X. Wang, G. Sheng, J. Fu, and Z. Zhou (2013), Mixing state of individual submicron carbon-containing particles during spring and fall seasons in urban Guangzhou, China: A case study, *Atmos. Chem. Phys.*, *13*(9), 4723–4735.
- Zhang, R. Y., A. F. Khalizov, J. Pagels, D. Zhang, H. X. Xue, and P. H. McMurry (2008), Variability in morphology, hygroscopicity, and optical properties of soot aerosols during atmospheric processing, *Proc. Natl. Acad. Sci. U.S.A.*, *105*(30), 10,291–10,296.
- Zhu, J., P. A. Crozier, and J. R. Anderson (2013), Characterization of light-absorbing carbon particles at three altitudes in East Asian outflow by transmission electron microscopy, *Atmos. Chem. Phys.*, *13*(13), 6359–6371.